

# Supporting Information

## Spectro-temporal Characterization of the Photoactivation Mechanism of Two New Oxidized Cryptochrome/Photolyase Photoreceptors

Johanna Brazard,<sup>†</sup> Anwar Usman,<sup>†</sup> Fabien Lacomat,<sup>†</sup> Christian Ley,<sup>†</sup>  
Monique M. Martin,<sup>†</sup> Pascal Plaza,<sup>\*†</sup> Laetitia Mony,<sup>§</sup> Marc Heijde,<sup>‡</sup>  
Gérald Zabulon,<sup>‡</sup> and Chris Bowler<sup>‡</sup>

<sup>†</sup> UMR 8640 CNRS-ENS-UPMC, Département de Chimie, Ecole Normale Supérieure,  
24 rue Lhomond, 75005 Paris, France

<sup>§</sup> UMR 8601 CNRS, Laboratoire de Chimie et Biochimie Pharmacologies et  
Toxicologiques, Université Paris Descartes,  
12 rue de l'École de médecine, 75006 Paris, France

<sup>‡</sup> UMR 8186 CNRS-ENS, Département de Biologie, Ecole Normale Supérieure,  
46 rue d'Ulm, 75005 Paris, France

### CONTENTS

1. Spectroscopic chemical analysis of MTHF and FAD in OtCPF2
2. Total concentration of FAD and concentration of MTHF in OtCPF2
3. Global analysis of the transient absorption data of OtCPF1
4. Global analysis of the transient absorption data of OtCPF2
5. Reconstructed isotropic transient spectra of OtCPF2
6. SVD analysis of the polarized transient spectra of OtCPF2
7. Photoreduction products of OtCPF1
8. Homology modeling
9. Ground-state heterogeneity of OtCPF2
10. Photoreduction products of OtCPF2

### 1. Spectroscopic chemical analysis of MTHF and FAD in OtCPF2

The presence of FAD, as opposed to FMN or ribloflavin, in OtCPF2 was evidenced by steady-state fluorescence spectroscopy. The emission intensity of the supernatant obtained after heat denaturation increases by a factor of five upon lowering the pH from 8.0 to 3.0 (see Figure S1A). This effect is characteristic of FAD.<sup>1</sup>

After treatment of OtCPF2 by sodium borohydride (NaBH<sub>4</sub>), its fluorescence spectrum shows the disappearance of the peak at 493 nm (see Figure S1B) assigned to MTHF. This is due to the reduction, hence loss, of MTHF by NaBH<sub>4</sub>.<sup>2</sup>

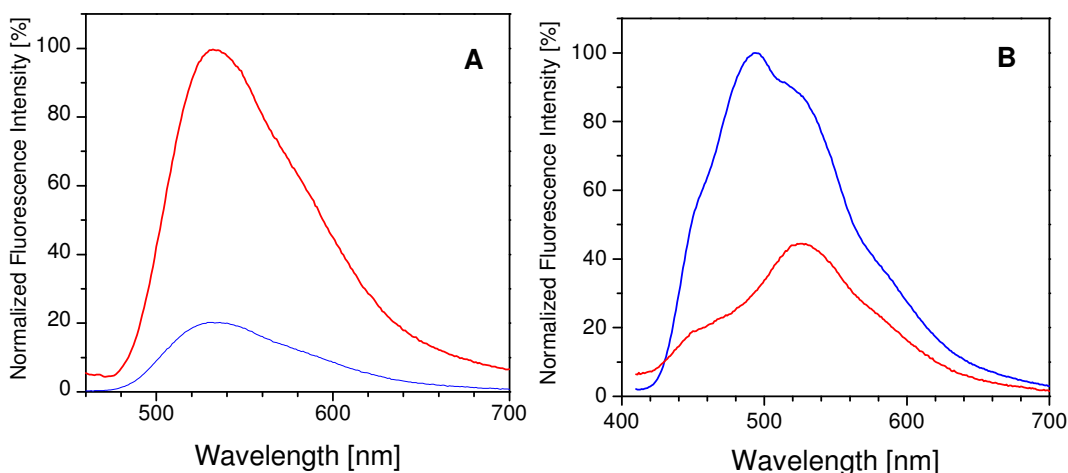


**Figure S1.** A: steady-state normalized fluorescence spectra ( $\lambda_{\text{ex}} = 450 \text{ nm}$ ) of the flavin released from the protein upon heat denaturation at pH 8.0 (blue) and at pH 3.0 (red). B: steady-state fluorescence spectra ( $\lambda_{\text{ex}} = 400 \text{ nm}$ ) of OtCPF2 in Tris buffer, before (blue) and after (red) treatment by  $\text{NaBH}_4$ .

## 2. Total concentration of FAD and concentration of MTHF in OtCPF2

After heat denaturation, the steady-state absorption spectrum of the supernatant of OtCPF2 was globally fitted with a sum of the absorption spectra of free  $\text{FAD}_{\text{ox}}$ ,<sup>3</sup> and of hydrolyzed MTHF at pH 8.0 (10-FTHF).<sup>4,5</sup> The fit gives the total concentration of FAD and the concentration of MTHF.

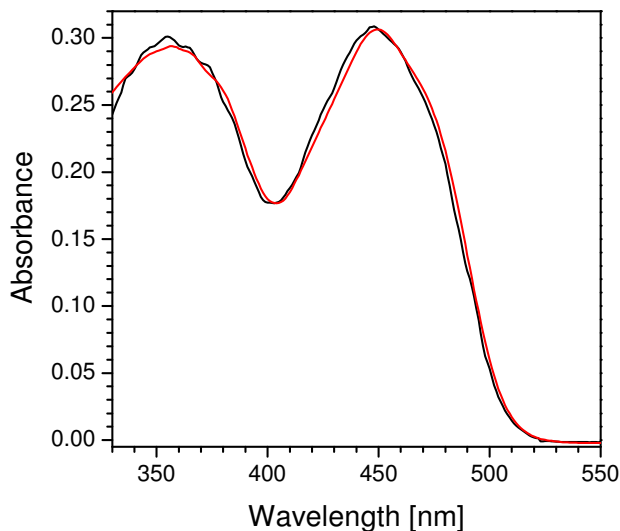


**Figure S2.** Steady-state absorption spectrum of OtCPF2 in Tris buffer (black) after heat denaturation and corresponding best fit (red) obtained with the sum of free  $\text{FAD}_{\text{ox}}$ ,<sup>3</sup> and 10-FTHF.<sup>4,5</sup>

### 3. Global analysis of the transient absorption data of OtCPF1

Global kinetic analysis of the time-resolved transient absorption data of OtCPF1 was best performed by using three exponential components plus a plateau. The lifetimes of the exponentials were found to be:  $0.39 \pm 0.03$  ps,  $9 \pm 2$  ps, and  $81 \pm 8$  ps. The respective preexponential factors DADS (Decay-Associated Difference Spectra) are given in Figure S3A.

DADS1 is negative in the stimulated-emission band, which indicates the excited-state decay of  $\text{FAD}_{\text{ox}}$ , while it is close to zero in the bleaching band, which confirms that nearly no recovery of the ground state occurs during the first kinetic step. DADS2 is close to zero between 370 and 450 nm and shows a large positive band between 493 and 750 nm. DADS3 and DADS4 are negative in the bleaching band, in agreement with a partial recovery of the ground state. The others contributions are all positive.

The Evolution-Associated Difference Spectra (EADS; see definition in the main text, Section 2.3) calculated from the present global analysis are presented in Figure S3B.

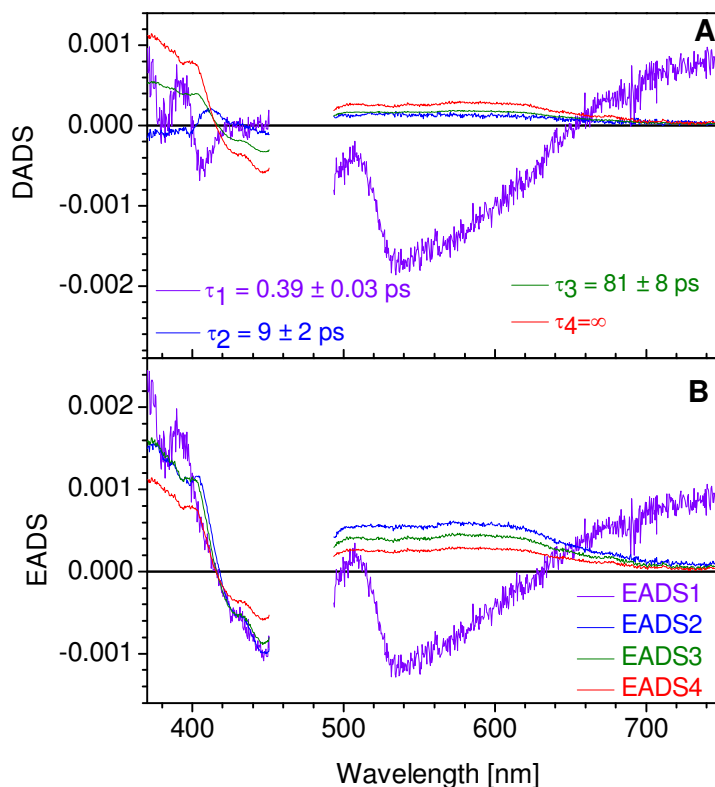


**Figure S3.** A: DADS attached to each of the four time components found in the global analysis of the transient absorption spectra of OtCPF1, recorded under excitation at 470 nm and isotropic conditions. B: Corresponding Evolution-Associated Difference Spectra (EADS).

### 4. Global analysis of the transient absorption data of OtCPF2

The time-resolved transient absorption data of OtCPF2 were globally fitted to a sum of three exponential components plus a plateau. The lifetimes of the exponentials were

found to be:  $0.59 \pm 0.03$  ps,  $13 \pm 3$  ps, and  $340 \pm 43$  ps. The corresponding DADS are represented in Figure S4A.

DADS1 shows the loss of the stimulated-emission band, corresponding to the decay of the excited-state of  $\text{FAD}_{\text{ox}}$ . A small negative amplitude is seen in the bleaching band area, potentially showing that a small part of the excited state population relaxes to the ground-state during the first kinetic step. This bleaching loss is not observed in the transient spectra of Figure 4A (main text), likely because convolution by the set-up response function partially obscures the initial dynamics, whereas DADS1 is calculated with the deconvoluted data. The amplitude of DADS2 is small, negative in the bleaching domain and a positive everywhere else. It is important to notice a shallow dip around 540 nm which evokes the loss of a stimulated emission contribution. DADS3 has negative contributions only in the bleaching area, which is the signature of a partial ground-state recovery. DADS3 is otherwise positive, with a broad band extending from 500 to 650 nm. DADS4 is non homothetic with DADS3: it has a negative amplitude in the bleaching area and a positive one beyond 495 nm. The latter transient absorption band shows low local maxima around 500 and 600 nm.

The EADS calculated from the present global analysis are presented in Figure S4B.

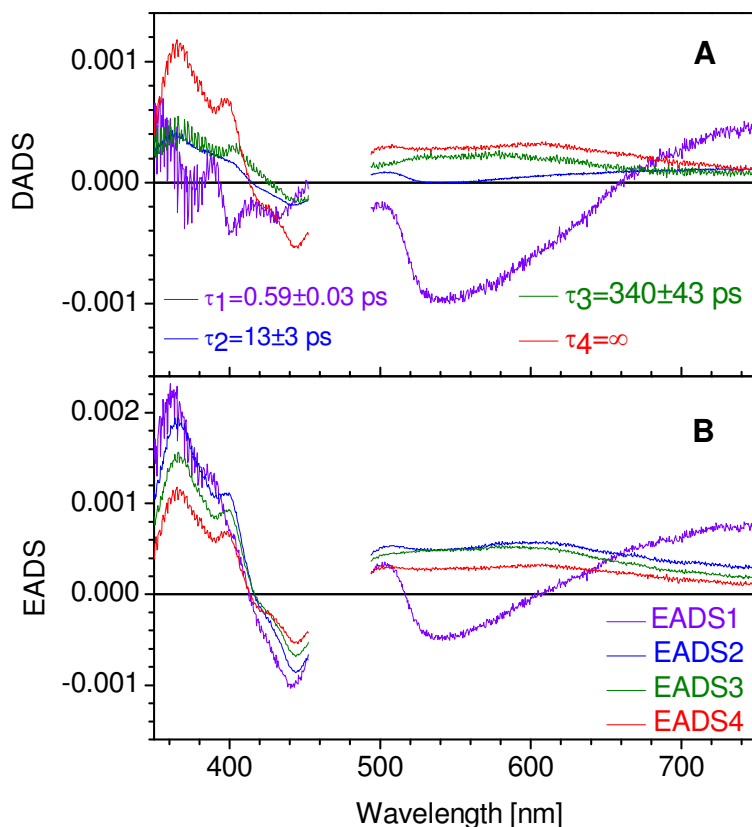


**Figure S4.** A: DADS attached to each of the four time components found in the global analysis of the transient absorption spectra of OtCPF2, recorded under excitation at 470 nm and isotropic conditions. B: Corresponding Evolution-Associated Difference Spectra (EADS).

## 5. Reconstructed isotropic transient spectra of OtCPF2

The validity of the polarized transient absorption spectra was checked by reconstructing the isotropic transient spectra defined as:

$$\Delta A^{\text{iso}} = \frac{\Delta A_{\parallel} + 2 \times \Delta A_{\perp}}{3}$$

The reconstructed isotropic spectra are shown in Figure S5. They are very similar to those directly measured for OtCPF2-Iso (see main text, Figure 4).

Global analysis performed of those reconstructed spectra yielded the following time constants:  $0.41 \pm 0.05$  ps,  $8 \pm 2$  ps, and  $334 \pm 63$  ps. They are in good agreement with those found for the isotropic data:  $0.59 \pm 0.03$  ps,  $13 \pm 3$  ps, and  $340 \pm 43$  ps.

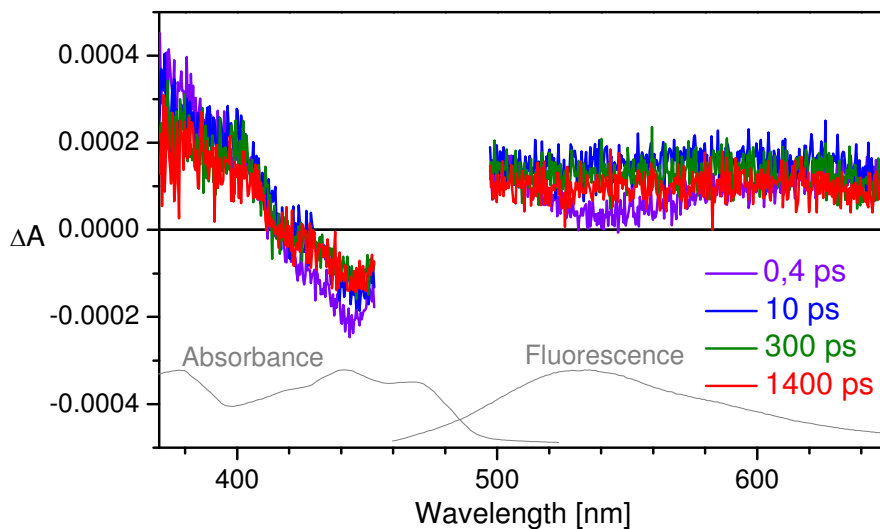


**Figure S5.** Reconstructed isotropic transient absorption spectra of OtCPF2-Aniso in Tris buffer, measured after excitation at 470 nm.

## 6. SVD analysis of the polarized transient spectra of OtCPF2

We performed a simultaneous global analysis of the parallel and perpendicular transient absorption data of OtCPF2 (see main text, Section 3.4). The best fit was obtained with the same fit function as for the isotropic data, i.e. three exponentials plus a plateau. The exponential lifetimes were found to be:  $0.46 \pm 0.05$  ps,  $9 \pm 2$  ps and  $301 \pm 50$  ps, in close agreement with those found under isotropic conditions. The corresponding DADS and EADS are given in Figure S6 and S7, respectively. Spectra numbering follows increasing order of the lifetimes.

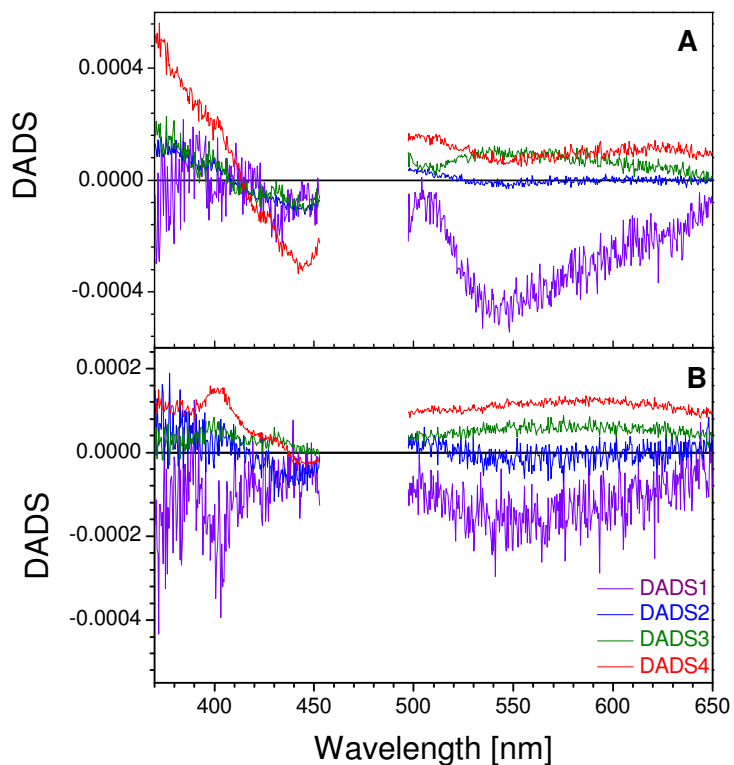


**Figure S6.** DADS attached to each of the four time components found in the simultaneous global analysis of the polarized transient absorption spectra of OtCPF2, recorded after excitation at 470 nm under parallel (A) and perpendicular (B) conditions.

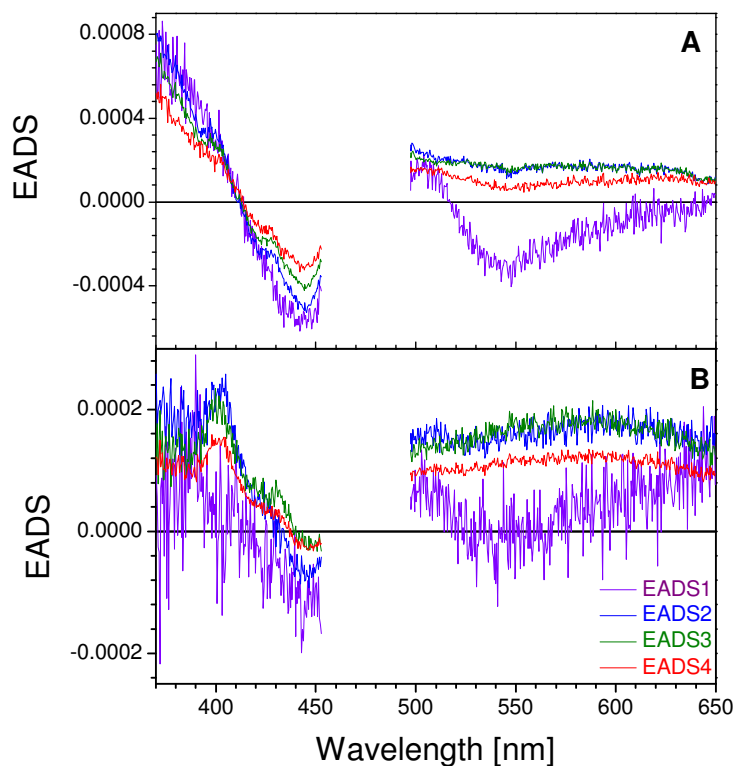


**Figure S7.** EADS calculated in the simultaneous global analysis of the polarized transient absorption spectra of OtCPF2, recorded after excitation at 470 nm under parallel (A) and perpendicular (B) conditions.

## 7. Photoreduction products of OtCPF1

Figure S8 compares the reconstructed transient absorption spectrum of the  $\text{FAD}^{\bullet-}/\text{WH}^{\bullet+}$  pair (main text, Figure 7A) with the experimental transient absorption spectrum of OtCPF1 measured once the photoinduced reaction occurring in 390 fs is over (EADS2 from Figure S3B was used instead of any raw spectrum in order to improve S/N ratio). Both spectra have been normalized at 450 nm. Although the spectra are not quite superimposed, their resemblance indicates that the photoproducts formed during the first kinetic step are very likely the  $\text{FAD}^{\bullet-}$  and  $\text{WH}^{\bullet+}$  radicals. The mismatches could in part be due to our insufficient knowledge of the real spectra of the different radicals inside OtCPF1 and in part to the fact that other species than  $\text{FAD}_{\text{ox}}$  were excited in this experiment (5%  $\text{FADH}^{\bullet*}$ , 7%  $\text{FADH}^{\bullet*}$ ) and may contribute to the data.

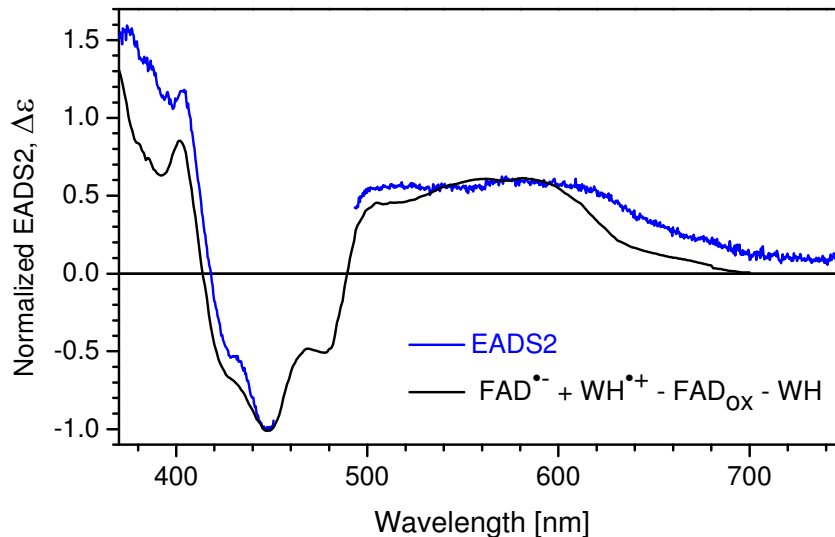


**Figure S8.** Comparison of the EADS2 of OtCPF1 (blue) and the reconstructed difference spectrum ( $\Delta\epsilon$ ) for  $\text{FAD}^{\bullet-}/\text{WH}^{\bullet+}$  (black) after normalization at 450 nm.

## 8. Homology modeling

The alignments of the OtCPF1 and OtCPF2 protein sequences (Protein ID: CAL53781.1 and CAL50547.1, respectively) were generated with the online software ClustalW2 (EBI, <http://www.ebi.ac.uk/Tools/clustalw2/index.html>). These alignments were further manually refined according to predicted (OtCPF1 and OtCPF2) and known (reference sequences, see below) secondary structures. The secondary elements of OtCPF1 and OtCPF2 were predicted from their primary structure by using PROF predictions (<http://www.predictprotein.org/>).<sup>6</sup>

OtCPF1 was aligned on the sequences of three 6-4 photolyases (Dm64 from *Drosophila melanogaster*, Protein ID: AAL90322.1; Xl64 from *Xenopus laevis*, ID: NP\_001081421; Ds64 from *Dunaliella salina*, ID: AAX56342.1), two CDP photolyases (EcCPD from *Escherichia coli*, ID: NP\_415236.1; AnCPD from *Anacystis nidulans*, ID: YP\_399131.1) and one cryptochrome DASH (AtCry3 from *Arabidopsis thaliana*, ID: NP\_568461.2).

OtCPF2 was aligned on the sequences of five cryptochromes DASH (AtCry3; DrDASH from *Danio rerio*, ID: NP\_991249.1; XlDASH from *Xenopus laevis*, ID: NP\_001084438; SynDASH from *Synechocystis* sp. PCC6803, ID: NP\_441086.1; VcDASH from *Vibrio cholerae*, ID: ZP\_01981240.1), one 6-4 photolyase (Dm64), one CPD photolyase (EcCPD), and one cryptochrome (AtCry1 from *Arabidopsis thaliana*, ID: AAM70572.1).

Figure S9A shows the part of the alignments that demonstrates the conservation of the tryptophan chain across the CPF family. For simplicity only the sequences of OtCPF1, OtCPF2, Dm64, AtCry3 and EcCPD are represented.

Homology models were subsequently generated by the automated comparative modeling tool MODELER 9.0,<sup>7</sup> in the DS Modeling 1.7 framework (Accelrys, San Diego, CA). Models were generated according to the previously generated alignment, and by using the coordinates of Dm64 (PDB code: 3CVU) for OtCPF1 and AtCry3 (PDB: 2IJG)

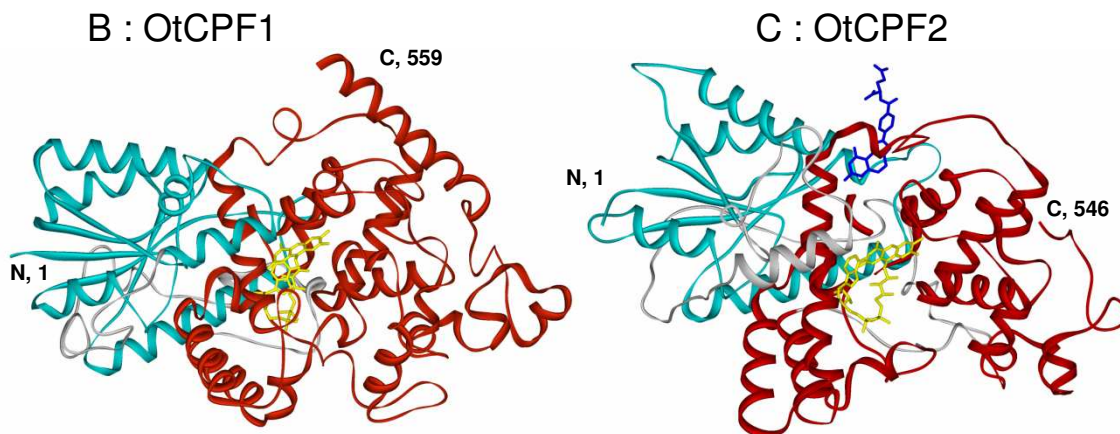
for OtCPF2. The structural quality of the models was assessed with MODELER 9.0 probability density functions and with Profiles-3D analysis (in DS Modeling 1.7). These models were initially generated and optimized in presence of FADH<sub>2</sub> for both proteins and with MHF for OtCPF2. MHF (5,10-methenyl-6,7,8-trihydrofolic acid) is a close parent of MTHF found in the crystal structure of AtCry3. The final models obtained with FAD<sub>ox</sub> (Figures S9B and S9C) were generated after changing the oxidation and protonation states of FAD and optimizing the amino acids surrounding FAD (within a radius of 1 nm) by using the CHARMM calculation engine (within DS Modeling 1.7).<sup>8</sup>

**A**

	α11	α12	α13	α14	
OtCPF1	TSLMGQLMWREFYYLVAA--G	TKNFKDMEGNAICRQIFPKKDR	ELFAAWENAQTGFPPWIDAAMTQLR	REGWLHHLARHAV	414
OtCPF2	YWMIFELIWRDFFKFFALKHGNKIFH-LDG-TAGRRASAKRDEKILKAWKTGTTGYPLIDANMRELAATGFMSNRGRQNV				392
Dm64	VSLIGQLMWREFYYTVAA--AEPNFDRLGNVYCMQIIPQDEHPDHLEAWTHGRTGYPFIDAIMRQLRQEGWIHHLARHAV				394
AtCry3	YWVLFELIWRDYFRFLSIKCGNSLFH-LGG-PRNVQGKMSQDQKLFESWRDAKTGYPLIDANMKELSTTGFMNSNRGRQIV				398
EcCPD	SVWLNELIWRFEYRHLITYHPSLCKHRPFI-AWTRVQMSNPAHLQAWQEGKTYPIVDAAMRQLNSTGWMHNLRLRMIT				347

	α15	α16	α17	α18	
OtCPF1	ACFLTRGDLFIHTEWGRDAFDRDLVDADWALNNGNMMWLSL---	SAFFYQYFRVYSPIAFAKKYDKDGQYVRHYLPVLKN			491
OtCPF2	ASWLAL-DAGIDWRHGADWFEHLLDYDTASNWGNWCAAAGMTGG-RI---	NR-FNIAKQTKDYDPAGEYIKTWVKELAE			466
Dm64	ACFLTRGDLWISIEEGQRVFEQLLLDQDWALNAGNMMWLSA---	SAFFHQYFRVYSPVAFGKKTDPQGHYIRKYVPELSK			471
AtCry3	CSFLVLR-DMGLDWRMGAEFWFETCLLDYDPCSNYGNMITYGAGVGNDPRE---	DRYFSIPKQAQNYDPEGEYVAFWLQQLRR			474
EcCPD	ASFLVK-DLLIDWRREGERYFMSQLIDGDLAANNGGQWAASTGTDAAAP--	YFRIFNPTTQGEKFDHEGEFIRQWLPELRD			424



**Figure S9.** A: Sequence alignment of OtCPF1 and OtCPF2 with Dm64, AtCry3 and EcCPD in the region containing the three conserved tryptophan residues, highlighted in yellow boxes, involved in the electronic transfer. In red are indicated  $\alpha$ -helices ( $\beta$ -strands are not visible in this region) either predicted (OtCPF1, OtCPF2) or found from known X-ray structures (Dm64, AtCry3, EcCPD). B,C: 3D structure of OtCPF1 (B) and OtCPF2 (C) as calculated by homology modeling. FAD<sub>ox</sub> is shown in yellow and MHF in blue.

## 9. Ground-state heterogeneity of OtCPF2

As mentioned in the main text (Section 4.2.1) the transient absorption spectra of OtCPF2 are similar to those of OtCPF1. The DADS attached to the 13 ps component (DADS2) however exhibits a dip around 540 nm which may be assigned to the loss of

stimulated emission, that is, a signature of excited-state decay. Three hypotheses can be put forward to explain it:

- Hypothesis 1: during first 0.59 ps step two reactions would compete. One of them would be the photoreduction of excited  $\text{FAD}_{\text{ox}}$  and second one the partial photorelease of  $\text{FAD}_{\text{ox}}$  to the solvent. DADS2 would then be the signature of the released excited  $\text{FAD}_{\text{ox}}$ , decaying in 13 ps. Free  $\text{FAD}_{\text{ox}}$  in its closed conformation is known to decay in 5-20 ps in solution.<sup>9-14</sup>
- Hypothesis 2: an equilibrium would exist between excited  $\text{FAD}_{\text{ox}}$  (state 1) and a reaction product (state 2), which in turn would yield other photoproducts.
- Hypothesis 3: the OtCPF2 sample is heterogeneous and contains two populations of  $\text{FAD}_{\text{ox}}$ . The first one undergoes photoreduction in 0.59 ps; it is called the reactive population. The second one does not undergo photoreduction and just decays in 13 ps; it is called the non-reactive population.

$\text{FAD}_{\text{ox}}$  has many interactions with different amino acids of the protein.<sup>15</sup> It therefore seems unlikely that  $\text{FAD}_{\text{ox}}$  could be released from OtCPF2 in 0.59 ps and hypothesis 1 was not retained. In hypothesis 2, state 1 would decay in 0.59 ps and 13 ps, and state 2 would rise in 0.59 ps and decay in 13 ps. DADS2 should have two positive contributions (decays) from states 1 and 2 and one negative signature from state 2 (rise). Although this kinetic model cannot be excluded, its interpretation seems too complex to us at the moment, and we did not develop it further. Since hypothesis 3 is simple and plausible, we retained it even if we could not establish its uniqueness.

Within hypothesis 3, the non-reactive population would contribute to DADS2 only; which does not exclude that the reactive population could also contribute to it. The fact that both populations would share a common lifetime would have to be considered as a coincidence or an artifact due to the global analysis being unable to discriminate between too close time components.

Let us first suppose that only the non-reactive population contributes to DADS2 and examine the nature of this non-reactive  $\text{FAD}_{\text{ox}}$ . The maximum of the stimulated-emission band of DADS2 is blue shifted as compared to the one of free  $\text{FAD}_{\text{ox}}$  in solution.<sup>12,16</sup> In addition, the bleaching band of DADS2 is narrower and more structured than that of free  $\text{FAD}_{\text{ox}}$  in solution. These observations allow one to discard the possibility that the non-reactive population would be free  $\text{FAD}_{\text{ox}}$  in solution. It means on the contrary that this population is likely still bound to the protein. This conclusion is supported by the fact that DADS2 bears a clear resemblance with the initial differential spectrum of the reactive population, which can be represented by the sum DADS1+DADS3+DADS4 (called EADS1'; not shown) within our present set of hypotheses. We tentatively propose that non-reactive  $\text{FAD}_{\text{ox}}$  could be bound to OtCPF2 in the binding site of MTHF, which is left free in 49% of the proteins in our purified samples (see main text, Section 3.1).

In the main text (Sections 3.2 and 4.1) the lifetime of 9 ps found for OtCPF1 (which is close to the 13 ps lifetime of OtCPF2) has been assigned to an electron transfer following the initial photoreduction of  $\text{FAD}_{\text{ox}}$ . If one assumes that the reactive  $\text{FAD}_{\text{ox}}$  of OtCPF2 may also contribute to DADS2, one would thus describe DADS2 as the sum of two terms: rDADS2 coming from the reactive population, and nrDADS2 arising from the non-reactive population. We tried to crudely decompose DADS2 into such a sum by taking nrDADS2 proportional to EADS1' (with proportionality factor  $\alpha$ ), standing for a typical excited-state spectrum of a bound, non-reacting,  $\text{FAD}_{\text{ox}}$ . Choosing  $\alpha = 0.135$

allows making rDADS2 look quite similar to DADS3 (see Figure S10), which has been identified as belonging to the dynamics of the reactive population (main text, Section 4.2). This rough decomposition is to be taken as indicative only but conveys the idea that DADS2 might contain contributions from reactive  $\text{FAD}_{\text{ox}}$ .

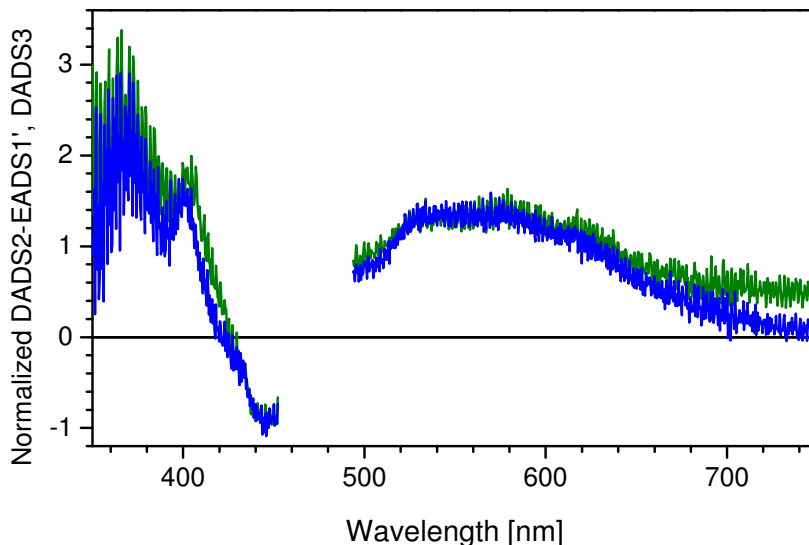


**Figure S10.** DADS3 of OtCPF2 (green) and the construction of  $\text{DADS2} - 0.135 \times \text{EADS1}'$  (blue) after normalization at 447 nm.

## 10. Photoreduction products of OtCPF2

In Figure S11, the reconstructed spectrum of  $\text{FAD}^{\bullet-}/\text{WH}^{\bullet+}$  is compared to the EADS3 of OtCPF2.

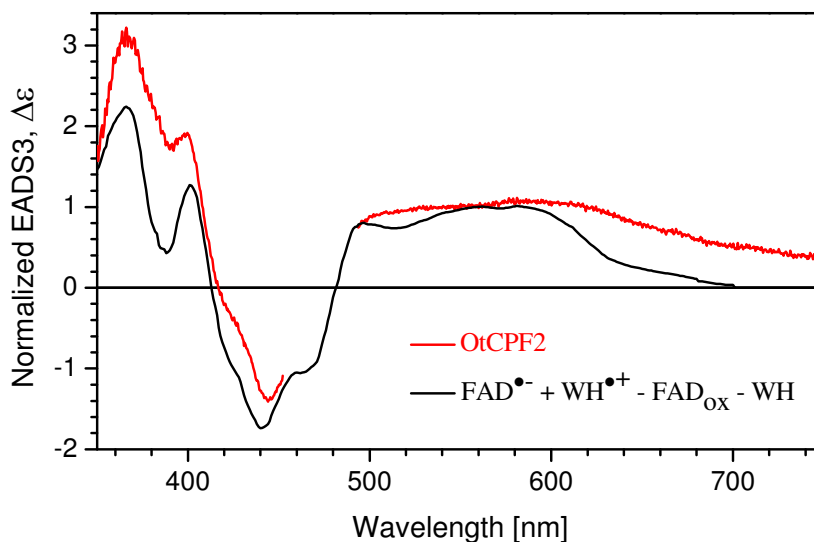


**Figure S11.** EADS3 of OtCPF2 (red) and the reconstructed difference spectra of  $\text{FAD}^{\bullet-}/\text{WH}^{\bullet+}$  (black) after normalization at 580 nm.

Although the spectra are not quite superimposed, their resemblance indicates that the photoproducts formed during the first two kinetic steps of OtCPF2 (0.59 and 13 ps) are very likely the  $\text{FAD}^{\bullet-}$  and  $\text{WH}^{\bullet+}$  radicals. As mentioned for OtCPF1, the differences might be due to the contribution of other excited species (5%  $\text{FADH}^{\bullet*}$ , 10%  $\text{FADH}^-$  and 7%  $\text{MTHF}^*$ ).

### Supporting References

- (1) Faeder, E. J.; Siegel, L. M. *Anal. Biochem.* **1973**, *53*, 332-336.
- (2) Hamm-Alvarez, S.; Sancar, A.; Rajagopalan, K. V. *J. Biol. Chem.* **1989**, *264*, 9649-9656.
- (3) Song, S. H.; Dick, B.; Penzkofer, A.; Pokorny, R.; Batschauer, A.; Essen, L. O. *J. Photochem. Photobiol. B* **2006**, *85*, 1-16.
- (4) Kay, L. D.; Osborn, M. J.; Hatefi, Y.; Huennekens, F. M. *J. Biol. Chem.* **1960**, *235*, 195-201.
- (5) May, M.; Bardos, T. J.; Barger, F. L.; Lansford, M.; Ravel, J. M.; Sutherland, G. L.; Shive, W. *J. Am. Chem. Soc.* **1951**, *73*, 3067-3075.
- (6) Rost, B.; Sander, C. *J. Mol. Biol.* **1993**, *232*, 584-599.
- (7) Sali, A.; Blundell, T. L. *J. Mol. Biol.* **1993**, *234*, 779-815.
- (8) Brooks, B. R.; Bruccoleri, R. E.; Olafson, B. D.; States, D. J.; Swaminathan, S.; Karplus, M. *J. Comput. Chem.* **1983**, *4*, 187-217.
- (9) Chosrowjan, H.; Taniguchi, S.; Mataga, N.; Tanaka, F.; Visser, A. *Chem. Phys. Lett.* **2003**, *378*, 354-358.
- (10) Kao, Y. T.; Saxena, C.; He, T. F.; Guo, L. J.; Wang, L. J.; Sancar, A.; Zhong, D. P. *J. Am. Chem. Soc.* **2008**, *130*, 13132-13139.
- (11) Kondo, M.; Nappa, J.; Ronayne, K. L.; Stelling, A. L.; Tonge, P. J.; Meech, S. R. *J. Phys. Chem. B* **2006**, *110*, 20107-20110.
- (12) Li, G. F.; Glusac, K. D. *J. Phys. Chem. A* **2008**, *112*, 4573-4583.
- (13) Stanley, R. J.; IV, A. W. M. *J. Phys. Chem. A* **2000**, *104*, 6899-6906.
- (14) van den Berg, P. A. W.; Feenstra, K. A.; Mark, A. E.; Berendsen, H. J. C.; Visser, A. *J. Phys. Chem. B* **2002**, *106*, 8858-8869.
- (15) Park, H. W.; Kim, S. T.; Sancar, A.; Deisenhofer, J. *Science* **1995**, *268*, 1866-1872.
- (16) Weigel, A.; Dobryakov, A. L.; Veiga, M.; Lustres, J. L. P. *J. Phys. Chem. A* **2008**, *112*, 12054-12065.